Structural Admissibility in Crystallographic Phase Chains and Polymorph Ladders

UNNS Substrate Research Program

March 22, 2026

Abstract

We report a crystallography-focused empirical study of structural admissibility in ordered crystalline matter using the STRUC-I v1.0.4 chamber. The corpus consists of eight materials represented as descriptor ladders derived from canonical crystal structures: three ferroic perovskite systems ($BaTiO_3$, $PbTiO_3$, $KNbO_3$), three oxide polymorph systems (TiO_2, ZrO_2, SiO_2), a single-phase oxide control (Al_2O_3), and a metallic structural pair (Fe). For each material a common descriptor family is extracted: lattice parameters a, b, and c, cell volume, volume per atom, and volume per formula unit, yielding 48 ladders across six descriptor channels.

Across 1,920 κ-step evaluations no violation of the admissibility inequality

$$\mathrm{inv}(P_\varepsilon;\, L) \;\le\; \nu(V_\varepsilon(L))$$

was observed. The global minimum admissibility rate is $A_\kappa = 0.9835$ ($KNbO_3$ volume-per-formula-unit at $\kappa = 1$). Five ladders enter Weak Persistence: four from SiO_2 ($\bar{\rho} = 0.423$–0.499) and one from $KNbO_3$ (cell-volume channel, $\bar{\rho} = 0.362$). No ladder enters the Boundary-Stabilized regime.

The SiO_2 c-axis ladder ($\bar{\rho} = 0.499$) establishes a new maximum for ordered non-biological matter in the analyzed STRUC-I corpus, exceeding the prior condensed-matter maximum of $\bar{\rho} = 0.424$ (Si density). Two-state systems (Fe, $PbTiO_3$) anchor the minimal non-degenerate pressure regime near $\bar{\rho} \approx 0.009$, while Al_2O_3 realises the degenerate zero-vulnerability limit.

These results extend the admissibility map of the Universal Structural Law from property ladders to crystallographic phase-linked structures and show that admissibility in crystalline matter is comparative rather than merely binary: real phase chains and polymorph ladders remain within admissible bounds, but different structural families load pressure into different descriptor channels according to the severity and symmetry of their geometric reorganization.

1. Introduction

The question addressed in this paper is whether crystallographic phase chains and polymorph families, when represented as ordered descriptor ladders, remain admissible under perturbation. Crystalline matter is a natural setting for this question. Crystals are formally specified, symmetry-constrained, experimentally measurable ordered structures with standardized public data, natural orderable quantities, and clear perturbative interpretation. If a domain-general admissibility principle governs realizable ordered systems, crystallography is one of the clearest settings in which it should appear.

This paper extends recent multi-domain admissibility analyses [1] to the crystallographic setting. That framework establishes the admissibility inequality as an empirical constraint across

more than 3,000 physical ladder evaluations spanning thirteen domains, with condensed matter previously represented by DFT-computed density, formation-energy, and band-gap property ladders. The present study does not re-establish the broader result. It asks whether the same admissibility logic extends from ordered property ladders to crystallographic phase chains and polymorph progressions, and adds a qualitatively new class of ordered objects to the empirical map.

Phase-linked systems and polymorph series are stronger candidates than generic ordered datasets because they probe the boundary between structural persistence and transformation. They test not only whether admissibility holds, but how structural pressure is redistributed as ordered matter undergoes nontrivial reorganization. The corpus was designed to address three questions that property ladders alone cannot answer:

(i) Does admissibility survive the discrete phase-chain representation, in which ladder rungs correspond to distinct crystallographic phases rather than continuous property values?

(ii) Does the framework distinguish between isostructural phase progressions that carry different degrees of geometric distortion—such as the formally identical four-state ferroic sequences of $BaTiO_3$ and $KNbO_3$?

(iii) Does structural pressure rank polymorph families in a way that tracks the known severity of their network-topological reorganization?

The present corpus supports affirmative answers to all three questions.

The corpus was assembled as a compact reference set rather than a large uncontrolled archive. The design principle was breadth of structural role with minimal redundancy: three ferroic phase chains, three oxide polymorph systems, one single-phase control, and one metallic pair. The results resolve a clear hierarchy of pressure regimes and establish the first Weak Persistence instances from non-biological ordered matter that arise from geometric phase reorganization rather than from property-space clustering.

2. Relation to Prior Work

This study is a crystallography-specific extension of earlier multi-domain admissibility analyses [1, 2], in which condensed matter was previously represented by DFT-computed property ladders for ten material families. In those analyses the prior condensed-matter maximum was $\bar{\rho} = 0.424$ (Si density, $n = 42$).

The phase-chain corpus differs from the property-ladder corpus in a fundamental structural respect. Property ladders order a large collection of related compounds by a single continuously-valued physical property; phase-chain ladders order a small set of symmetry-distinct phases of the same material by a structural descriptor, so that each ladder rung corresponds to a qualitatively different crystal structure. The two representations probe different aspects of the admissibility geometry: property ladders test a continuous distribution of descriptor values across a material family; phase-chain ladders test the gap structure induced by discrete symmetry-breaking transitions.

Both representations satisfy the admissibility inequality. The phase-chain corpus raises the observed pressure ceiling for ordered non-biological matter within the analyzed dataset, and provides a structurally differentiated picture that is not available from property ladders alone. In particular, it occupies a region of the admissibility landscape between relaxed physical systems and the more stressed biological regimes reported in [1**?**].

3. Admissibility Framework

The following definitions specialise the general framework of [1] to the crystallographic context.

Definition 1 (Crystallographic descriptor ladder)**.** *A* crystallographic descriptor ladder *is a finite ordered sequence $L = (x_1, \ldots, x_n)$ constructed from a physically meaningful structural descriptor extracted across a phase chain, polymorph family, or tightly defined comparison set of canonical crystal structures. The elements x_i are values of a single descriptor for n distinct crystallographic phases, sorted ascending.*

Definition 2 (Perturbative admissibility)**.** *Given a perturbation protocol P_ε acting on ladder L with scale $\varepsilon = \kappa \cdot \delta_{\text{med}}$ (δ_{med} is the median gap of L, $\kappa \in [0.01, 1.0]$), let $\text{inv}(P_\varepsilon; L)$ denote the expected inversion count and $\nu(V_\varepsilon(L))$ denote the vulnerability capacity (maximum independent set of the vulnerability graph $V_\varepsilon(L)$).*

Definition 3 (Structural pressure)**.** *The* structural pressure index *is*

$$\rho \;=\; \frac{\text{inv}}{\nu},$$

and the mean structural pressure $\bar{\rho}$ *is the average of $\rho(\kappa)$ over the κ-grid. Low $\bar{\rho}$ indicates a relaxed admissible ladder; elevated $\bar{\rho}$ indicates proximity to the admissibility boundary.*

Definition 4 (Structural classification states)**.** *Following the STRUC-I v1.0.4 protocol, ladders are assigned to one of three states:*

- Stable Structure*: $A_\kappa = 1.000$ and $\bar{\rho} < \theta_{\text{WP}}$.*
- Weak Persistence*: $A_\kappa < 1.000$ or $\bar{\rho} \geq \theta_{\text{WP}}$.*
- Boundary-Stabilized*: $A_\kappa < 1.000$ and $\bar{\rho} \geq \theta_{\text{BS}}$ with $\theta_{\text{BS}} > \theta_{\text{WP}}$.*

Remark 1. *The inequality is treated empirically rather than axiomatically. The objective is not to derive a theorem from crystallographic first principles, but to test whether real phase-linked crystal families satisfy the inequality when translated into descriptor ladders. The combinatorial basis of the inequality—specifically, that admissibility holds whenever inversion events embed as an independent set of the vulnerability graph [1] (Theorems 3–6 therein)—applies directly to the hierarchically-gapped gap spectra produced by crystallographic phase progressions.*

4. Corpus Construction

4.1. Design and material selection

The corpus was assembled as a compact reference set. Eight materials were selected across four structural categories:

- *Ferroic phase chains*: $BaTiO_3$, $PbTiO_3$, $KNbO_3$;
- *Canonical polymorph systems*: TiO_2, ZrO_2, SiO_2;
- *Single-phase oxide control*: Al_2O_3;
- *Metallic structural pair*: Fe.

$BaTiO_3$ provides the reference standard for a four-state ferroic progression. $PbTiO_3$ provides a minimal two-state ferroic check. $KNbO_3$ extends the ferroic side into a four-state chain that, as the results show, loads substantially more pressure into volumetric channels than $BaTiO_3$ despite sharing the same nominal phase order. TiO_2, ZrO_2, and SiO_2 represent canonical polymorph oxide systems with successively more severe structural reorganizations. Al_2O_3 is a single-state control (corundum baseline). Fe is a metallic BCC/FCC pair.

4.2. Phase representatives and descriptor extraction

Canonical crystallographic representatives were identified from standard crystal entries using symmetrized CIF files sourced from the Materials Project [4]. Table 1 summarises the phase representatives.

Table 1: Phase representatives. Space groups in standard Hermann–Mauguin notation. n: number of phases.

Material	**Phase sequence**	n	**Structural role**
Al_2O_3	Corundum ($R\bar{3}c$)	1	Single-phase control
Fe	BCC ($Im\bar{3}m$) $\rightarrow$ FCC ($Fm\bar{3}m$)	2	Metallic pair
$PbTiO_3$	Tetrag. ($P4mm$) $\rightarrow$ Cubic ($Pm\bar{3}m$)	2	Minimal ferroic pair
TiO_2	Rutile ($P4_2/mnm$) $\rightarrow$ Anatase ($I4_1/amd$) $\rightarrow$ Brookite ($Pbca$)	3	Polymorph oxide
ZrO_2	Mono. ($P2_1/c$) $\rightarrow$ Tetrag. ($P4_2/nmc$) $\rightarrow$ Cubic ($Fm\bar{3}m$)	3	Polymorph oxide
SiO_2	Quartz ($P3_121$) $\rightarrow$ Tridymite ($C222_1$) $\rightarrow$ Cristobalite ($Fd\bar{3}m$)	3	Polymorph oxide
$BaTiO_3$	Rhomb. ($R3c$) $\rightarrow$ Ortho. ($Amm2$) $\rightarrow$ Tetrag. ($P4mm$) $\rightarrow$ Cubic ($Pm\bar{3}m$)	4	Ferroic chain
$KNbO_3$	Rhomb. ($R3c$) $\rightarrow$ Ortho. ($Amm2$) $\rightarrow$ Tetrag. ($P4mm$) $\rightarrow$ Cubic ($Pm\bar{3}m$)	4	Ferroic chain

The common descriptor family extracted for each material is:

$$a, \quad b, \quad c, \quad \text{cell volume}, \quad \text{volume per atom}, \quad \text{volume per formula unit}.$$

4.3. Descriptor validation and ladder preparation

Descriptor extraction and ladder conversion were validated against the accepted STRUC-I input schema. Each ladder was checked for descriptor consistency, ordering integrity, and chamber-readable formatting before final evaluation. The single-phase Al_2O_3 control provided an internal consistency check of the degenerate limit, yielding zero structural pressure across all six channels as expected for $n = 1$.

4.4. Instrument settings

All evaluations used the standard preregistered STRUC-I v1.0.4 protocol: $\kappa \in [0.01, 1.0]$, $K = 40$ logarithmically spaced steps, $M = 2{,}000$ Monte Carlo draws per κ-step, and perturbation scale $\varepsilon = \kappa \cdot \delta_{\text{med}}$. The corpus contains 48 ladders and 1,920 κ-step evaluations. No parameters were adjusted post-hoc.

5. Results

5.1. Primary result

Observation 1 (Zero violations)**.** *Every ladder in the corpus satisfies the admissibility inequality throughout the tested perturbation range. Across 48 ladders and 1,920 κ-step evaluations, the violation count is zero. The crystallographic phase-chain domain is empirically non-falsifying under STRUC-I.*

This result is non-trivial because the corpus spans qualitatively different crystallographic roles: a single-phase control, two-state comparisons, four-state ferroic chains, and polymorph systems involving substantially different geometric rearrangements. The zero-violation outcome is not guaranteed by the construction itself and appears to depend on the gap architecture of the physical crystal structures represented here.

Figure 1 shows the full per-descriptor pressure profile for all eight materials. The overall hierarchy and the Weak Persistence cases (filled diamonds) are immediately visible.

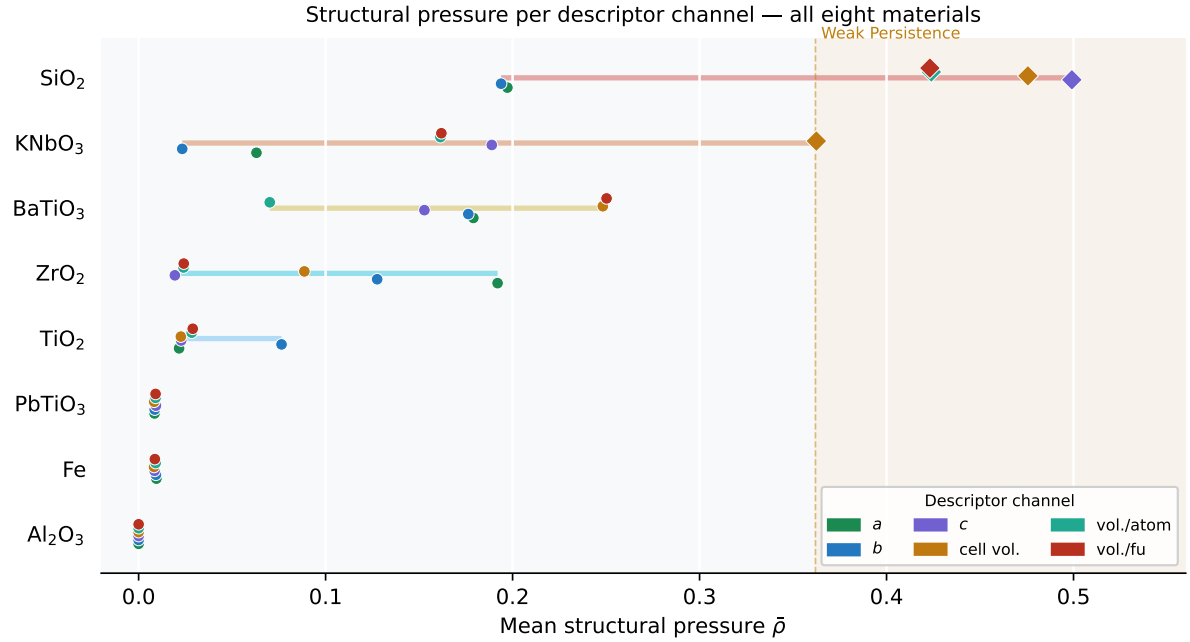

Figure 1: Structural pressure landscape for all eight materials. Each row shows one material. Coloured circles give $\bar{\rho}$ for each of the six descriptor channels (see legend); horizontal bars span the per-material range. Filled diamonds indicate Weak Persistence classification. The shaded region marks $\bar{\rho} \geq 0.362$, the lowest Weak Persistence value in the corpus ($KNbO_3$ cell volume). Al_2O_3 is not shown because $\bar{\rho} = 0$ on all channels.

Table 2 gives the per-material summary.

5.2. Full per-ladder results

Table 3 gives complete numerical results for all 48 ladders.

Table 2: Per-material corpus summary. n: phases. $\bar{\rho}$ range: min to max mean structural pressure across six descriptor channels. Min A_κ: worst-case admissibility rate. WP: Weak Persistence ladders out of six.

Material	n	$\bar{\rho}$ range	Min A_κ	WP	**Worst state**
Al_2O_3	1	0.000	1.0000	0	Stable (degenerate)
Fe	2	0.008–0.010	1.0000	0	Stable Structure
$PbTiO_3$	2	0.008–0.009	1.0000	0	Stable Structure
TiO_2	3	0.022–0.076	1.0000	0	Stable Structure
ZrO_2	3	0.019–0.192	1.0000	0	Stable Structure
$BaTiO_3$	4	0.070–0.250	0.9945	0	Stable Structure
$KNbO_3$	4	0.023–0.362	0.9835	1	Weak Persistence
SiO_2	3	0.194–0.499	1.0000	4	Weak Persistence
All	–	0.000–0.499	0.9835	5	0 violations

Table 3: Complete per-ladder results. $\bar{\rho}$: mean pressure. $\rho_{\max}$: maximum pressure. $\rho(\kappa{=}1)$: pressure at largest perturbation scale. A_κ: minimum admissibility rate. WP = Weak Persistence; Stable = Stable Structure.

Material	**Descriptor**	$\bar{\rho}$	$\rho_{\max}$	$\rho(\kappa{=}1)$	A_κ	**State**
Al_2O_3	a	0.000	0.000	0.000	1.0000	Stable
Al_2O_3	b	0.000	0.000	0.000	1.0000	Stable
Al_2O_3	c	0.000	0.000	0.000	1.0000	Stable
Al_2O_3	cell volume	0.000	0.000	0.000	1.0000	Stable
Al_2O_3	volume/atom	0.000	0.000	0.000	1.0000	Stable
Al_2O_3	volume/fu	0.000	0.000	0.000	1.0000	Stable
Fe	a	0.0095	0.132	0.132	1.0000	Stable
Fe	b	0.0093	0.137	0.137	1.0000	Stable
Fe	c	0.0085	0.117	0.117	1.0000	Stable
Fe	cell volume	0.0083	0.123	0.123	1.0000	Stable
Fe	volume/atom	0.0091	0.128	0.128	1.0000	Stable
Fe	volume/fu	0.0087	0.125	0.125	1.0000	Stable
$PbTiO_3$	a	0.0085	0.117	0.117	1.0000	Stable
$PbTiO_3$	b	0.0086	0.131	0.131	1.0000	Stable
$PbTiO_3$	c	0.0093	0.128	0.128	1.0000	Stable
$PbTiO_3$	cell volume	0.0083	0.123	0.123	1.0000	Stable
$PbTiO_3$	volume/atom	0.0091	0.128	0.128	1.0000	Stable
$PbTiO_3$	volume/fu	0.0091	0.123	0.123	1.0000	Stable
TiO_2	a	0.0216	0.277	0.277	1.0000	Stable
TiO_2	b	0.0764	0.363	0.363	1.0000	Stable
TiO_2	c	0.0228	0.265	0.265	1.0000	Stable
TiO_2	cell volume	0.0226	0.264	0.264	1.0000	Stable
TiO_2	volume/atom	0.0284	0.292	0.292	1.0000	Stable

Table 3 continued.

Material	Descriptor	$\bar{\rho}$	$\rho_{\max}$	$\rho(\kappa{=}1)$	A_κ	State
TiO_2	volume/fu	0.0290	0.279	0.279	1.0000	Stable
ZrO_2	a	0.192	0.451	0.448	1.0000	Stable
ZrO_2	b	0.128	0.424	0.424	1.0000	Stable
ZrO_2	c	0.0194	0.259	0.259	1.0000	Stable
ZrO_2	cell volume	0.0886	0.402	0.402	1.0000	Stable
ZrO_2	volume/atom	0.0240	0.282	0.282	1.0000	Stable
ZrO_2	volume/fu	0.0241	0.263	0.263	1.0000	Stable
$BaTiO_3$	a	0.179	0.434	0.290	1.0000	Stable
$BaTiO_3$	b	0.176	0.435	0.303	1.0000	Stable
$BaTiO_3$	c	0.153	0.416	0.296	1.0000	Stable
$BaTiO_3$	cell volume	0.248	0.467	0.293	1.0000	Stable
$BaTiO_3$	volume/atom	0.070	0.455	0.455	0.9945	Stable
$BaTiO_3$	volume/fu	0.250	0.453	0.303	1.0000	Stable
$KNbO_3$	a	0.063	0.444	0.444	0.9980	Stable
$KNbO_3$	b	0.023	0.193	0.193	1.0000	Stable
$KNbO_3$	c	0.189	0.437	0.342	1.0000	Stable
$KNbO_3$	cell volume	0.362	0.496	0.372	1.0000	WP
$KNbO_3$	volume/atom	0.161	0.548	0.548	0.9875	Stable
$KNbO_3$	volume/fu	0.162	0.567	0.567	0.9835	Stable
SiO_2	a	0.197	0.464	0.463	1.0000	Stable
SiO_2	b	0.194	0.465	0.465	1.0000	Stable
SiO_2	c	0.499	0.518	0.512	1.0000	WP
SiO_2	cell volume	0.476	0.512	0.485	1.0000	WP
SiO_2	volume/atom	0.424	0.518	0.484	1.0000	WP
SiO_2	volume/fu	0.423	0.504	0.496	1.0000	WP

5.3. Degenerate and minimal-pressure limits

Al_2O_3 yields $\rho = 0$ across all six descriptor ladders: the degenerate zero-vulnerability limit expected for $n = 1$. The result serves as an internal consistency check confirming that the instrument correctly handles the single-phase edge case.

The minimal non-degenerate regime is occupied by Fe and $PbTiO_3$. Both lie near $\bar{\rho} \approx 0.008$–0.009 across all six descriptors, consistent with the behaviour expected of a two-state system with a single gap: only one vulnerability window exists, so inversion pressure remains minimal while the structure remains nontrivial. The near-identical $\bar{\rho}$ values confirm that chain length is the primary determinant of pressure at this end of the spectrum, irrespective of whether the system is metallic or ferroic.

5.4. Ferroic pressure hierarchy

The ferroic trio shows a systematic internal hierarchy. $PbTiO_3$ sits at the minimal non-degenerate end. $BaTiO_3$, with its four-state rhombohedral → orthorhombic → tetragonal → cubic sequence, remains fully admissible but rises to $\bar{\rho}$ up to 0.250 in the cell-volume and volume-per-formula-unit channels. $KNbO_3$, which follows the formally identical four-state phase sequence, loads

substantially more pressure into volumetric channels, with the cell-volume ladder entering Weak Persistence at $\bar{\rho} = 0.362$.

Observation 2 (Isostructural discrimination)**.** *$BaTiO_3$ and $KNbO_3$ share the same nominal ferroic phase sequence yet produce measurably different structural pressures. The cell-volume pressure differential $\Delta\bar{\rho} = 0.362 - 0.248 = 0.114$ quantifies the greater geometric anisotropy of the $KNbO_3$ lattice distortions across the same phase order.*

This finding illustrates the comparative character of the admissibility analysis. The framework does not simply classify all four-state ferroic chains as Stable. It distinguishes between isostructural progressions according to the admissibility cost carried by each descriptor channel.

5.5. Polymorph pressure hierarchy

The oxide polymorph systems show a sharper ordering:

$$\mathrm{TiO_2} \ll \mathrm{ZrO_2} \ll \mathrm{SiO_2}.$$

TiO_2 (rutile/anatase/brookite) remains deeply relaxed, $\bar{\rho} \in [0.022, 0.076]$, all Stable. ZrO_2 (monoclinic/tetragonal/cubic) reaches $\bar{\rho}$ up to 0.192, all Stable. SiO_2 (quartz/tridymite/cristobalite) is substantially more stressed, with four of six descriptor ladders entering Weak Persistence and the c-axis ladder reaching $\bar{\rho} = 0.499$.

Observation 3 (Polymorph ranking)**.** *The ordering $TiO_2 \ll ZrO_2 \ll SiO_2$ tracks the known crystallographic severity of the underlying reorganization. TiO_2 polymorphs remain within rutile-like framework space, differing principally in octahedral tilting. ZrO_2 introduces a stronger monoclinic distortion with significant bond-angle changes. SiO_2 moves between tetrahedral frameworks with substantially different network topologies—six-membered rings in quartz, four-membered rings in cristobalite—the most radical transformation in the corpus. The framework ranks these families in a way that tracks this crystallographic hierarchy.*

Although four of the six SiO_2 ladders enter Weak Persistence, all record $A_\kappa = 1.0000$ and no ladder approaches the Boundary-Stabilized regime. Elevated $\bar{\rho}$ reflects structural stress, not structural failure.

Figure 2 shows the $\rho(\kappa)$ profiles for both material groups. The left panel displays mean curves for the three ferroic systems; the right panel shows per-descriptor curves for SiO_2 alongside the mean curves for TiO_2 and ZrO_2.

5.6. Descriptor-channel anisotropy

A pattern cuts across materials rather than between them. In multi-phase systems, volumetric descriptors—cell volume, volume per atom, and volume per formula unit—tend to carry higher structural pressure than axial descriptors a, b, and c. The principal exception is SiO_2, where the c-axis ($\bar{\rho} = 0.499$) is anomalously elevated and becomes the highest-pressure ladder in the corpus, while a and b remain Stable at $\bar{\rho} \approx 0.194$–0.197. Table 4 summarises the anisotropy per material.

This anisotropy shows that the instrument responds to structured geometric load rather than producing a flat material-wide label. A material can remain fully admissible while concentrating its structural stress into a single channel. For crystallography, this makes the analysis more than a binary admissibility test: it becomes a comparative diagnostic of where the admissibility cost of structural reorganization is paid.

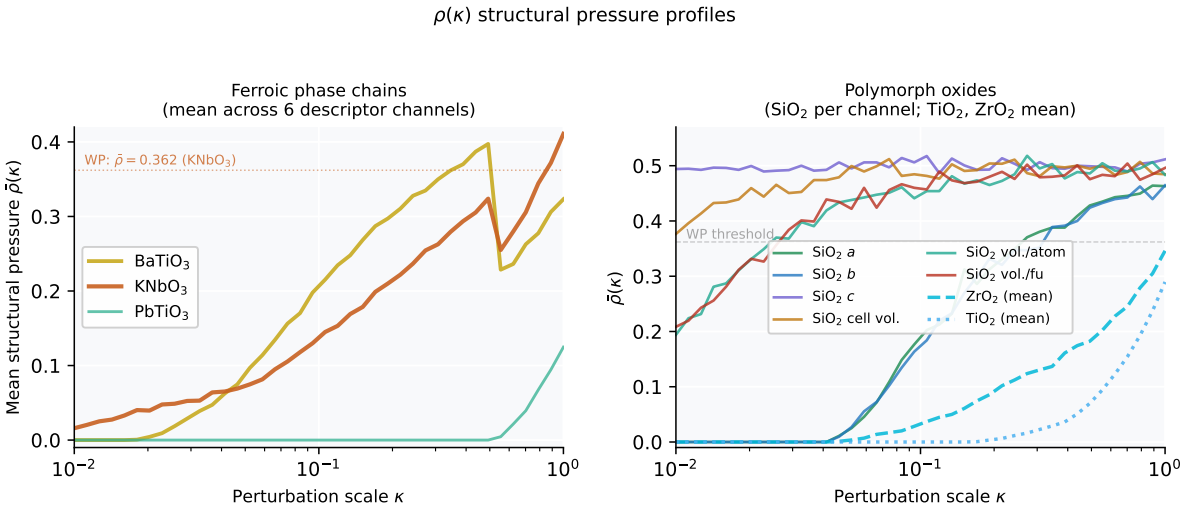

Figure 2: Structural pressure $\rho(\kappa)$ as a function of perturbation scale κ (log scale). *Left*: mean $\rho(\kappa)$ across all six descriptor channels for each ferroic system. $KNbO_3$ rises above the dashed reference line (Weak Persistence onset at $\bar{\rho} = 0.362$) across much of the perturbation range. *Right*: per-descriptor curves for SiO_2 (solid, coloured by descriptor channel) together with the mean curves for TiO_2 (dotted) and ZrO_2 (dashed). The SiO_2 c-axis channel (purple) and volumetric channels (amber, teal, red) reach or exceed the Weak Persistence threshold.

Table 4: Descriptor-channel pressure anisotropy. $\Delta\bar{\rho} = \bar{\rho}_{\max} - \bar{\rho}_{\min}$ across the six channels.

Material	$\bar{\rho}_{\min}$	$\bar{\rho}_{\max}$	$\Delta\bar{\rho}$	**High-pressure channel**
$BaTiO_3$	0.070 (volume/atom)	0.250 (volume/fu)	0.180	volumetric
$KNbO_3$	0.023 (b)	0.362 (cell volume)	0.339	cell volume
SiO_2	0.194 (b)	0.499 (c)	0.305	c-axis
ZrO_2	0.019 (c)	0.192 (a)	0.173	a-axis
TiO_2	0.022 (a)	0.076 (b)	0.054	b-axis (minor)
Fe	0.008 (cell volume)	0.010 (a)	0.002	isotropic
$PbTiO_3$	0.008 (cell volume)	0.009 (c)	0.001	isotropic

Figure 3 presents the complete $\bar{\rho}$ values as a descriptor–material heatmap, making the channel anisotropy and the contrast between material families simultaneously visible.

Remark 2. *The SiO_2 c-axis anomaly reflects a genuine crystallographic feature. In quartz the c-direction is the direction along which the tetrahedral helix runs; the quartz-to-tridymite-to-cristobalite progression involves the most dramatic changes in c-axis scaling relative to the other lattice parameters. The framework identifies this anisotropy quantitatively without requiring any domain-specific input about the underlying crystal chemistry.*

6. Position within the Wider Corpus

6.1. Pressure ceiling for ordered non-biological matter

In the earlier multi-domain analysis [1], the condensed-matter maximum was $\bar{\rho} = 0.424$ (Si density ladder). The present corpus raises that ceiling within the present corpus: the SiO_2 c-

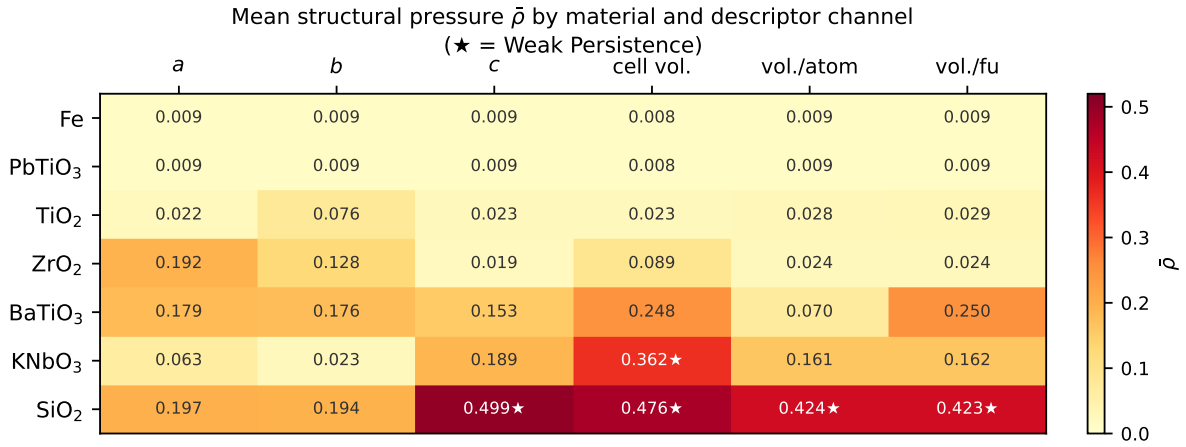

Figure 3: Mean structural pressure $\bar{\rho}$ for every material–descriptor combination. Cell values give $\bar{\rho}$ to three decimal places; cells marked $\star$ are classified Weak Persistence. The colour scale runs from white (zero pressure) to deep red (maximum). Al_2O_3 is omitted ($\bar{\rho} = 0$ on all channels). Volumetric channels (columns 4–6) consistently carry higher pressure than axial channels (columns 1–3), except in SiO_2 where the c-axis is anomalously elevated (top-right cluster).

axis ladder reaches $\bar{\rho} = 0.499$ and the cell-volume ladder reaches $\bar{\rho} = 0.476$, both fully admissible. This extends the admissibility map upward for ordered non-biological matter without entering the Boundary-Stabilized regime.

Table 5 positions the phase-chain results within the wider corpus.

6.2. Extension toward the degenerate limit

The corpus also extends the pressure map inward. Al_2O_3 confirms the degenerate limit at $\rho = 0$, while Fe and $PbTiO_3$ anchor the lowest non-degenerate pressures in the condensed-matter branch. Taken together, the phase-chain corpus spans approximately a 55-fold range in mean pressure, from Fe ($\bar{\rho} \approx 0.009$) to the SiO_2 c-axis ($\bar{\rho} = 0.499$), wider than any earlier single physical domain in the analyzed evidence base in absolute terms.

This crystallographic corpus adds 1,920 evaluations to the wider STRUC-I evidence base and introduces five additional Weak Persistence ladders without producing any clean violation.

7. Interpretation

Three conclusions follow from the corpus.

The law extends to phase-chain representations. Crystallographic phase chains and polymorph families satisfy the admissibility inequality. The result holds across a span of structural roles from the degenerate single-phase control to four-state ferroic chains and geometrically extreme polymorph sequences. The zero-violation outcome is consistent with the identification in [1] of hierarchical gap connectivity as the structural mechanism underlying admissibility: crystallographic phase progressions produce gap spectra that are hierarchically connected, not isolated block-degenerate.

Table 5: Phase-chain results in context. Domain means for non-crystallographic entries are from [1]; phase-chain values are from this study (shaded rows). All entries ordered by mean structural pressure.

Domain / Ladder	$\bar{\rho}$	A_κ	**State**
Solar coronal plasma (F10.7)	0.022	1.000	Stable
Earth gravity (EIGEN-6C4)	0.073	1.000	Stable
GOE n=100 (null baseline)	0.087	1.000	Stable
Fe BCC/FCC *(this study)*	0.009	1.000	Stable
$PbTiO_3$ *(this study)*	0.009	1.000	Stable
TiO_2, max channel *(this study)*	0.076	1.000	Stable
Molecular spectra (HITRAN mean)	0.115	1.000	Stable
GNSS crustal displacement (mean)	0.133	1.000	Stable
Nuclear γ-spectra (mean)	0.197	1.000	Stable
Condensed-matter DFT (mean)	0.204	$\geq$0.993	Stable–Weak
CMB Planck 2018 (mean)	0.254	1.000	Stable
$BaTiO_3$, max channel *(this study)*	0.250	0.9945	Stable
$KNbO_3$, cell volume *(this study)*	0.362	1.000	Weak Persistence
Solar dynamo (sunspot number)	0.376	$\approx$1.000	Weak Persistence
Si density (prior CM maximum)	0.424	0.9979	Weak Persistence
SiO_2, c-axis *(this study)*	**0.499**	1.000	**Weak Persistence**
Biology: combined deletion	0.554	0.9994	Weak Persistence
Biology: deletion (length-altering)	0.819	1.0000	Boundary-Stabilized

Admissibility is comparative, not merely binary. The meaningful result is not just that every ladder passes. The corpus differentiates sharply among material classes: TiO_2 is deeply interior; ZrO_2 is moderate; SiO_2 is high-pressure but fully admissible; $KNbO_3$ is the ferroic stress case; Fe and $PbTiO_3$ define the minimal non-degenerate regime; Al_2O_3 supplies the degenerate control. These distinctions emerge from the geometric properties of the descriptor ladders and are not imposed by the framework.

The framework localises where structural pressure lives. In this corpus the main load is typically carried by volumetric channels, with SiO_2 showing the clearest axial exception. This channel-specific reading transforms the admissibility analysis from a binary pass/fail test into a comparative diagnostic: a measurement of where the admissibility cost of structural reorganization is actually paid, and by extension, which descriptor channels may be most sensitive to approaching phase boundaries.

Observation 4 (Admissibility as comparative structural diagnostic)**.** *The phase-chain corpus establishes that ordered crystal families occupy different positions within the admissibility landscape according to (a) the number of phases in the progression, (b) the severity of the geometric reorganization across phases, and (c) the descriptor channel through which the reorganization is primarily expressed. The framework measures all three effects simultaneously via the per-channel $\bar{\rho}$ profile.*

8. Outlook

The natural extension of this work is the transition from static phase-linked ladders to parameterised structural trajectories. The present results point to a specific open question: whether structural pressure rises continuously as a material is driven toward a phase boundary and relaxes again after the transition.

A natural prediction suggested by these results is the following. Well inside a stable phase, continuous structural-parameter ladders (e.g., $a(T)$, $V(T)$ across a temperature scan) should lie deep in the Stable Structure regime. Approaching a transition, inversion pressure should rise as structural parameters converge toward near-degenerate values. Near criticality, the system may enter Weak Persistence, and the characteristic perturbation scale κ^* may shift as the gap spectrum acquires near-degenerate pairs. A first-order transition would be expected to produce a sharp reset in the ρ profile as the new phase re-establishes a well-separated gap spectrum.

The per-material $\bar{\rho}$ profiles and descriptor-channel anisotropies established here provide the calibrated reference-state signatures for testing these predictions. A phase-transition dynamics study would determine whether structural pressure rises predictably as a thermodynamic control parameter approaches a transition, transforming the admissibility framework from a static structural audit into a dynamical diagnostic of phase-boundary proximity.

9. Conclusion

This paper has presented a crystallography-focused empirical test of the admissibility inequality in ordered matter. The corpus contains eight materials, 48 descriptor ladders, and 1,920 chamber evaluations. No violation was observed. The global minimum admissibility rate was $A_\kappa = 0.9835$ ($KNbO_3$ volume-per-formula-unit), and no ladder entered the Boundary-Stabilized regime.

The stronger result is comparative. Crystallographic systems do not merely pass uniformly. They stratify by structural pressure. TiO_2 and ZrO_2 occupy relaxed and moderate admissible interiors. SiO_2 reaches $\bar{\rho} = 0.499$ on the c-axis channel—the highest value for ordered non-biological matter in the analyzed corpus—while remaining fully admissible. $KNbO_3$ loads substantially more volumetric pressure than $BaTiO_3$ despite sharing the same nominal ferroic phase order. Al_2O_3 verifies the degenerate limit, and Fe together with $PbTiO_3$ anchors the minimal non-degenerate regime.

The crystallographic analysis does more than confirm a known law in another domain. It sharpens the empirical content of the admissibility framework by showing that ordered crystal families occupy different positions within the admissibility landscape according to the severity and channel structure of their geometric reorganization. The SiO_2 result establishes that a geometrically extreme polymorph sequence—one involving radical changes in tetrahedral network topology—can approach the upper range of non-biological structural pressure while remaining fully admissible. This extends the empirical scope of the Universal Structural Law to one of the most structurally diverse regions of condensed matter and motivates future work on phase-boundary dynamics.

Data availability. All corpus ladder CSV files, STRUC-I v1.0.4 chamber outputs (JSON), and supporting analysis reports are available from the authors on request.
Instrument and protocol. CHAMBER STRUC-I v1.0.4. $\kappa \in [0.01, 1.0]$; 40 steps logspaced; $M = 2{,}000$ MC draws; $\varepsilon = \kappa \cdot \delta_{\text{med}}$; protocol preregistered; no parameters adjusted post-hoc.

References

[1] UNNS Substrate Research Program. The Universal Structural Law: Admissibility Bounds on Ordering Instability. *Manuscript*, v6, 2026.

[2] UNNS Substrate Research Program. STRUC-I v1.0.4 Corpus Analysis Report. *Internal technical report*, 2026.

[3] UNNS Substrate Research Program. STRUC-CONDMAT Corpus Analysis: Crystallographic Phase Chains and Polymorph Ladders. *Internal technical report*, 2026.

[4] A. Jain, S. P. Ong, G. Hautier, W. Chen, W. D. Richards, S. Dacek, S. Cholia, D. Gunter, D. Skinner, G. Ceder, and K. A. Persson. Commentary: The Materials Project: A materials genome approach to accelerating materials innovation. *APL Materials*, 1(1):011002, 2013. Data retrieved from the Materials Project next-generation explorer, https://next-gen.materialsproject.org/materials. UNNS Substrate Research Program. Admissibility Constraints Across Physical and Biological Systems. *Manuscript*, 2026.

References [2] and [3] are internal technical reports of the UNNS Substrate Research Program that document the computational instruments and corpus analyses supporting the results reported here.